*Geophys. J. Int.* (2008) **174,** 978–992 doi: 10.1111/j.1365-246X.2008.03865.x

# The shear-wave velocity structure in the upper mantle beneath Eurasia

B. Kustowski,[1,*] G. Ekström[2] and A. M. Dziewoński[1]

[1] *Department of Earth and Planetary Sciences, Harvard University, Cambridge, MA* 02138*, USA. E-mail: kustowski@post.harvard.edu*
[2] *Lamont-Doherty Earth Observatory of Columbia University, Palisades, NY* 10964*, USA*

Accepted 2008 May 24. Received 2008 May 9; in original form 2007 July 25

## SUMMARY

We develop an approach that allows us to invert for the mantle velocity structure within a finely parametrized region as a perturbation with respect to a low-resolution, global tomographic model. We implement this technique to investigate the upper-mantle structure beneath Eurasia and present a new model of shear wave velocity, parametrized laterally using spherical splines with $\sim$2.9° spacing in Eurasia and $\sim$11.5° spacing elsewhere. The model is obtained from a combined data set of surface wave phase velocities, long-period waveforms and body-wave traveltimes. We identify many features as narrow as few hundred kilometres in diameter, such as subducting slabs in eastern Eurasia and slow-velocity anomalies beneath tectonically active regions. In contrast to regional studies in which these features have been identified, our model encompasses the structure of the entire Eurasian continent. Furthermore, including mantle- and body-wave waveforms helped us constrain structures at depths larger than 250 km, which are poorly resolved in earlier models. We find that up to +9 per cent faster-than-average anomalies within the uppermost $\sim$200 km of the mantle beneath cratons and some orogenic regions are separated by a sharp gradient zone from deeper, +1 to +2 per cent anomalies. We speculate that this gradient zone may represent a boundary separating the lithosphere from the continental root, which might be compositionally distinct from the overlying lithosphere and remain stable either due to its compositional buoyancy or due to higher viscosity compared with the suboceanic mantle. Our regional model of anisotropy is not significantly different from the global one.

**Key words:** Tomography; Surface waves and free oscillations; Seismic tomography; Dynamics of lithosphere and mantle; Asia; Europe.



## 1 INTRODUCTION

The variety of tectonic provinces in the Eurasian continent makes it a challenging target for seismic tomography. Modelling seismic velocities beneath cratons that are far away from continental boundaries may help to understand the state of the lithosphere that is not affected by the flow in the suboceanic mantle. Studying regions of recent tectonic activity associated with the closing of the Tethys Ocean may provide insight into the processes of subduction and continental collision.

Different parts of Eurasia have been investigated extensively using forward modelling techniques and seismic tomography. Although imaging small portions of the continent may help to understand the local velocity structure, a continental-scale model is necessary for understanding differences between tectonic provinces and providing snapshots of large-scale geodynamic processes. A number of continental-scale models of North America and Australia have been developed; however, to date, only Shapiro & Ritzwoller (2002) presented a tomographic model encompassing the structure of the entire Eurasian continent, with regional-scale detail. Therefore, building a new, improved model of Eurasia should be important for better understanding of the structure and dynamics of the entire continent.

In this work, we develop a new model using a larger number of measurements of surface wave velocities than Shapiro & Ritzwoller (2002), which may potentially allow for resolving the structure in greater detail. We also include long-period waveforms that constrain velocities at depths larger than 250 km, which were not successfully modelled in the earlier model. Further differences include the implementation of a smooth, spline parametrization instead of a block parametrization, solving an inverse problem in the least-squares sense instead of searching the model space, and using a reference model STW105 (Kustowski *et al.* 2008), which is consistent with the data used in this study, instead of combination of PREM (Dziewonski & Anderson 1981) and ak135 (Kennett *et al.* 1995) used by Shapiro & Ritzwoller (2002).

*Now at: Chevron, 6001 Bollinger Canyon Road, D1136, San Ramon, CA 94583, USA.

There are several reasons why constructing a model of all of Eurasia is difficult. Direct arrivals of teleseismic body waves, which are often used in global tomography, are significantly sensitive to the upper-mantle structure only within a narrow cone beneath sources and receivers. Whereas ray path coverage for such data is fairly good in tectonically active regions, northern Eurasia is essentially aseismic, and the distribution of seismic stations is non-uniform and sparse. Measurements of body waves that are multiply reflected from the surface and turn in the upper mantle, provide important constraints on the upper-mantle structure in northern and central Eurasia (Grand & Helmberger 1985); however, these data have not been used to build a 3-D model of Eurasia. Observations of regional-distance body waves generated by nuclear and chemical explosions, which have been carried out in the former Soviet Union, sample the upper mantle beneath northern Eurasia and have been used to develop several compressional-wave velocity models (Ryberg *et al.* 1996; Morozova *et al.* 1999; Nielsen & Thybo 1999). These models are constructed along seismic profiles and are therefore only 2-D. Although the identification of triplicated arrivals in the 2-D case can be performed based on the careful analysis of data recorded along seismic profiles, the identification is difficult in the 3-D case (Garnero *et al.* 1992; Kustowski *et al.* 2003).

Surface waves provide more uniform data coverage than body waves. Tomographic inversions of surface wave measurements have been performed for several regions in Eurasia (e.g. Priestley & Debayle 2003; Boschi *et al.* 2004; Maggi & Priestley 2005). Development of a model of the entire Eurasia with the nominal resolution of 200–300 km, however, is computationally expensive as it involves ∼10 000–20 000 unknowns and large data sets necessary to constrain these unknowns.

In this work, we develop a new method that can be used to invert for a continental-scale model that consists of a fine grid of spherical splines superposed on a coarse global grid of splines. Such combined parametrization was previously implemented by Boschi *et al.* (2004) and Nettles & Dziewoński (2008). These authors, however, focused on the Mediterranean and North America, respectively, and inverted for anomalies associated with the fine and coarse parametrizations simultaneously. In contrast, we develop our model by inverting for the finely-parametrized structure in Eurasia as a perturbation with respect to a coarsely parametrized global model S362ANI (Kustowski *et al.* 2008). We choose this inversion strategy because it should allow for a more consistent comparison of different continental models than the simultaneous inversion. A potential pitfall of our iterative approach is that structures sensed by our global data set, which are not perfectly accounted for by the global model, will map into the regional model. However, Nettles (2005) showed that nearly all such errors should map into a narrow zone defined around the model region that will be interpreted.

The ability of surface wave tomography to resolve regional-scale velocity anomalies has been a subject of a vigorous debate. It has been suggested that small-scale velocity anomalies can be resolved properly only if finite-frequency effects are taken into account (e.g. Spetzler *et al.* 2002). Some more recent papers, however, indicate that effects of finite-frequency kernels are less significant (e.g. Trampert & Spetzler 2006). It may, therefore, be useful to explore empirically whether anomalies as small as ∼500 km in diameter, observed in our model, appear to be robust. We show here that such small-scale anomalies reduce data misfits and are well correlated with tectonic provinces, plate boundaries or have been reported in previous studies based on higher-frequency data.

Finally, our results may shed light on the debate regarding the thickness of fast-velocity anomalies beneath continents. Estimates of the depth extent of seismic signatures beneath continents range from 200 (e.g. Dziewonski 1971) to over 400 km (e.g. Jordan 1975). Our model suggests that different estimates may not necessarily be inconsistent with one another; a 200-km-thick layer of strong anomalies may be underlain by significantly weaker anomalies extending down to ∼400 km.

**Table 1.** Data used in this study.

| | No. of surface-wave phase anomalies |
|---|---|
| Love waves, $T = 35$ s | 58 405 |
| Love waves, $T = 37$ s | 58 405 |
| Love waves, $T = 40$ s | 59 152 |
| Love waves, $T = 45$ s | 59 340 |
| Love waves, $T = 50$ s | 81 766 |
| Love waves, $T = 60$ s | 83 859 |
| Love waves, $T = 75$ s | 83 904 |
| Love waves, $T = 100$ s | 79 430 |
| Love waves, $T = 150$ s | 55 510 |
| Rayleigh waves, $T = 35$ s | 162 715 |
| Rayleigh waves, $T = 37$ s | 162 715 |
| Rayleigh waves, $T = 40$ s | 163 574 |
| Rayleigh waves, $T = 45$ s | 164 148 |
| Rayleigh waves, $T = 50$ s | 203 982 |
| Rayleigh waves, $T = 60$ s | 206 560 |
| Rayleigh waves, $T = 75$ s | 206 487 |
| Rayleigh waves, $T = 100$ s | 199 559 |
| Rayleigh waves, $T = 150$ s | 160 470 |
| | **No. of long-period waveforms** |
| Body Waves $T > 50$ s | 19 117–22 522 |
| Mantle Waves $T > 125$ s | 16 440–24 101 |
| Mantle Waves $T > 200$ s | 939–1062 |
| | **No. of body-wave traveltimes** |
| *S, SS, ScS, ScSScS, SS-S, ScS-S, S-SKS, SKKS-SKS* | ∼84 000 |

*Note:* Phase anomalies of surface waves were measured using the method of Ekström *et al.* (1997), but the data set has been extended compared with the original paper. We use seismograms from the years 1994–2003 to build a set of 229 well-recorded $6.5 \leq M_w$ earthquakes. For great earthquakes, we analysed mantle waves with $T > 200$ s, and for smaller events we included mantle waves with $T > 125$ s and body waves with $T > 50$ s. Body-wave traveltimes were measured at Harvard and Scripps. In the right column, we show the number of surface wave and traveltime measurements and the ranges for the number of waveforms measured on the vertical, longitudinal and transverse components.

## 2 DATA AND MODELLING TECHNIQUE

### 2.1 Data

To invert for the new model S2.9EA of Eurasia, we use the same data set as in the inversion for the global model of shear wave velocity S362ANI (Kustowski *et al.* 2008). The data, which are listed in Table 1, consist of Love- and Rayleigh-wave phase velocities measured along 58 000–206 000 paths at nine periods between 35 and 150 s, mantle- and body-wave waveforms measured along ∼20 000 paths for each component and ∼84 000 teleseismic body-wave traveltimes. Compared with the inversion for the global model, we exclude only the measurements of *SS* precursors, which do not have enough resolving power to determine regional-scale variations in the depth of the transition zone discontinuities. Non-linear crustal effects were evaluated for CRUST2.0 (Bassin *et al.* 2000)

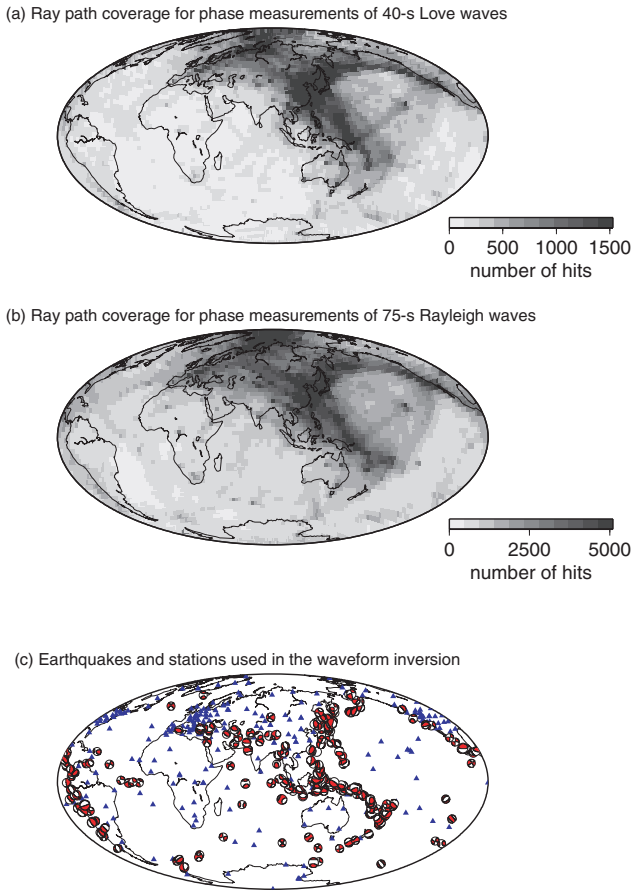


**Figure 1.** The ray path coverage for one of the smallest (a) and largest (b) sets of surface-wave phase measurements. The grey scale corresponds to the number of rays crossing each cell. The $3^\circ \times 3^\circ$ cells at the equator are comparable to the nominal resolution of the spherical-spline parametrization used in our model of Eurasia. The hit counts are corrected for different areas of the cells at different latitudes. In this work, we use only minor-arc observations. (c) Earthquakes (beach balls) and stations (triangles) used in the waveform inversion.

and subtracted from all data leaving them sensitive primarily to the velocity variations in the mantle. We weight particular data sets in the same way as in the inversion for a global model, that is, by selecting weights that allow for constraining radial basis function in the inversion at different depths as uniformly as possible.

Fig. 1 shows the number of rays crossing each $3^\circ \times 3^\circ$ cell for (a) one of the smallest and (b) one of the largest surface wave data sets. Surface wave phases were measured using the method of Ekström *et al.* (1997). Hit count maps show significantly better-than-average coverage in Eurasia, and we expect to resolve more details beneath this continent compared with other regions. Our collection of surface wave phases has been significantly expanded compared with the Ekström *et al.* (1997) data set, which was an important, but not the only, constraint on the mantle in the model of Shapiro & Ritzwoller (2002). Although fundamental-mode surface waves provide primary constraints on the structure of the uppermost 300 km of the mantle, it is essential to complement these data with long-period waveforms, measured using the method of Woodhouse & Dziewonski (1984), to determine shear wave velocities below 250–300 km. Structures at shallower depths can be fairly well resolved using only the overtone data, as shown by Ritsema *et al.* (2004); therefore, incorporating the overtones through the waveform inversion may also increase the resolution in the uppermost 300 km of the mantle. The contribution of our teleseismic body-wave traveltimes, measured using the cross-correlation techniques, is small since we invert only for the heterogeneity in the upper mantle.

### 2.2 Model parametrization

Fig. 2 shows knots of 1273 splines that we use to represent regional-scale lateral velocity perturbations in Eurasia with respect to a low-resolution global model S362ANI (Kustowski *et al.* 2008). The knots are approximately 2.9° apart from each other and cover the entire continent. Since we include our global data set in the inversion, it is necessary to account for the propagation effects outside of Eurasia. Such effects are predicted by the global model S362ANI, which was derived from the same data set that we use in this study. We subtract predictions of S362ANI from the observations and invert the residuals for the finer-scale perturbations in Eurasia.

The result of Nettles (2005) suggests that despite using a regional parametrization and a global data set, our inversion should be accurate as long as the high-resolution parametrization extends well beyond the region of interest that will be interpreted. Using the same type of parametrization and surface wave data as in our study, she compared the results of 2-D inversions in which the coefficients of low- and high-resolution splines were determined either simultaneously or iteratively as in our work. Nettles (2005) demonstrated that, although the simultaneous inversion is slightly more accurate, the modelling errors of the iterative inversion are small and located in a buffer zone outside of the region of interest. The shaded area in Fig. 2 and the area bound by the grey curve in Fig. 3 define our region of interest. The dense grid of 1273 splines extends beyond this region and consequently, perturbations are non-zero outside of this region. The zone of splines centred outside of the shaded region serves as a buffer zone defined in the same way as in Nettles (2005).

The advantage of using our iterative approach comes from the fact that it should allow for a more consistent comparison of different regional models than the simultaneous inversion. When the simultaneous inversion is performed, a new global model needs to be constructed for each regional model. Consequently, the comparison of two models of, for example, North America and Eurasia, would reflect not only differences between Eurasia and North America but also differences in the global models constructed in the inversions. If the global models were significantly different from each other, such comparison could not be used to discuss the true differences between the two continents. For example, if one global model showed stronger velocity gradients at a certain depth beneath all continents than the other global model, the comparison of the gradients beneath Eurasia and North America in the two models would be misleading. Building models of different continents on top of the same starting model would eliminate the dependence to the global inversions and make the comparison more sensitive to the true differences between the continents.

We choose to parametrize the model in terms of isotropic $\delta v_S = (\delta v_{SH} + \delta v_{SV})/2$ and radially anisotropic $\delta a_S = (\delta v_{SH} - \delta v_{SV})$ variations in shear wave velocity, as in the inversion for the global model S362ANI. This choice allows us to minimize the roughness of perturbations in both velocity and radial anisotropy. Our parametrization does not account for the azimuthal anisotropic variations, which are difficult to determine in a robust way (Larson *et al.* 1998). Ekström (2000) showed that trade-offs between isotropic and azimuthally anisotropic velocities are not significant in regions with good ray path coverage. Our data set has

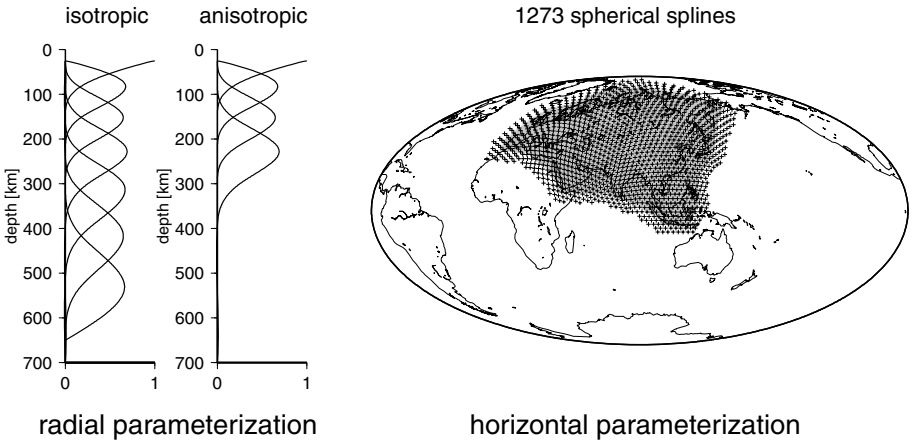


**Figure 2.** Geometrical parametrization of the high-resolution part of the model of Eurasia. Isotropic velocity perturbations $(\delta v_{SH}/v_{SH} + \delta v_{SV}/v_{SV})/2$ are represented in the vertical direction by seven B-splines in the upper mantle, whose amplitudes converge to zero at a depth of 650 km. Anisotropic perturbations $\delta v_{SH}/v_{SH} - \delta v_{SV}/v_{SV}$ are represented by four B-splines. Both isotropic and anisotropic perturbations are parametrized horizontally in terms of 1273 spherical splines, which are approximately 2.9° apart from each other. The shaded area in Eurasia defines the model region that is interpreted and is further discussed in the text. The parametrization of the global model is not shown in the figure.

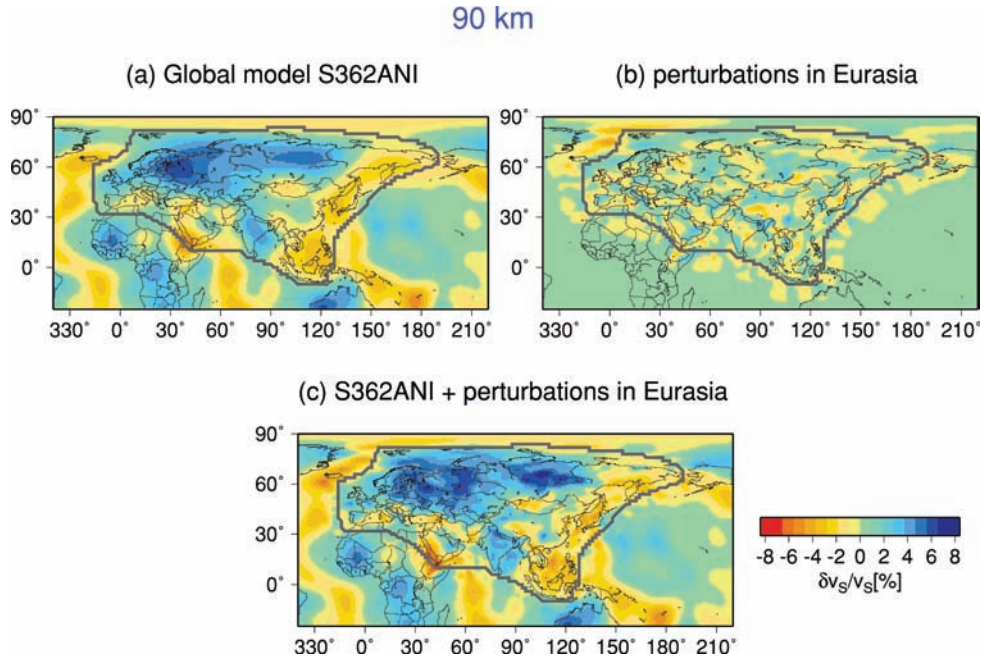


**Figure 3.** Isotropic velocity variations $(\delta v_{SH}/v_{SH} + \delta v_{SV}/v_{SV})/2$ at a depth of 90 km in Eurasia. (a) Variations in the low-resolution global model S362ANI. (b) High-resolution perturbations with respect to S362ANI obtained from eq. (4). (c) S2.9EA, that is, the sum of S362ANI and the high-resolution perturbations. The global average has been removed from the low-resolutions perturbations but not from the high-resolution perturbations. The grey line outlines the model region.

been expanded compared with that of Ekström (2000), and since the coverage in Eurasia is much better than the global average (Fig. 1), we do not expect that neglecting azimuthal anisotropy should lead to significant errors.

The global model S362ANI used as a starting model in our inversion is parametrized horizontally in terms of 362 spherical splines (Wang & Dahlen 1995; Wang *et al.* 1998) whose centres are approximately 11.5° apart from each other. Such coarse geometrical parametrization does not allow for resolving structures smaller than 1200 km. Imaging regional-scale features in Eurasia therefore requires higher nominal resolution, but the resolvable length-scale and the choice of the optimal parametrization depend on several factors. We choose a uniform parametrization throughout Eurasia with the nominal resolution of ∼300 km (Fig. 2). The motivation for this choice is the following.

The resolving power of the data is limited owing to the finite wavelength of seismic waves, theoretical approximations and noise. The resolution limits can be predicted theoretically, but estimates vary significantly. For example, Yoshizawa & Kennett (2002) find that the width of the zone of influence for a 40 s Rayleigh wave is ∼200 km and conclude that the resolution of tomographic images derived from rays crossing each other should be of the order of 300 km. Sieminski *et al.* (2004) also find that ray-based surface wave tomography can properly image regional-scale anomalies, given a

good data coverage. Spetzler *et al.* (2002), on the other hand, argue that, because of scattering effects, ray-theoretical surface wave tomography is limited to resolving anomalies larger than 1600 km for 40 s Love waves and 2700 km for 150 s Love waves. However, Boschi *et al.* (2004), using 35 s and longer-period Love and Rayleigh waves and ray theory, imaged anomalies of wavelengths shorter than 1000 km, which are consistent with high-resolution compressional-wave velocity models and tectonic reconstruction of the Mediterranean even at a depth of 250 km. Given that our data set is several times larger than that of Boschi *et al.* (2004), we expect to resolve heterogeneities of length-scales of a few hundred kilometres. Even if the resolving power of our data is not sufficiently good to determine anomalies as small as 300 km, the solution of the inverse problem should be robust. Boschi & Dziewonski (1999) showed that in regions of good data coverage, the roughness minimization of the overparametrized inverse problem leads to nearly identical results as using lower nominal resolution. We regularize the inverse problem by minimizing the horizontal and vertical roughness of the solution, and we show in Fig. 1 that our data coverage is very good. At all frequencies, at least 200 surface waves sample every $3^\circ \times 3^\circ$ block in Eurasia. The $3^\circ \times 3^\circ$ cells are equivalent to the nominal resolution implemented in our model. The number of ray paths for long-period waveforms is 3–10 times smaller than that for short- and intermediate-period surface waves but is still high. Therefore, we choose a simple, uniform parametrization in the entire region of interest. In fact, due to excellent data coverage, we were able to obtain a nearly identical model using norm damping.

Finally, our data cannot resolve details of the crustal structure, and we account for crustal effects by subtracting predictions of the *a priori* model CRUST2.0 (Bassin *et al.* 2000) from all our data. CRUST2.0 is defined on a $2^\circ \times 2^\circ$ grid. Because our shortest-period measurements have significant sensitivity to the crustal structure, the crustal model sets the limit for the resolution at 200 km.

We parametrize radial variations in the model using splines with the same spacing as in the global model. The knots of the radial splines are 50 km apart from each other just beneath the crust and 75 km apart from each other down to a depth of 300 km (Fig. 2). Radial parametrizations with the Mohorovičić discontinuity (hereafter Moho) depth varying according to CRUST2.0 have been implemented in inversions that involved only surface wave phase velocities, but accounting for such variations is computationally unfeasible when waveforms are included. To remedy this limitation, Marone & Romanowicz (2007) incorporated a simplified model with five distinct depths of the Moho. However, lateral velocity anomalies in a model with (Nettles & Dziewoński 2008) and without (Kustowski *et al.* 2008) the Moho depth variations are highly correlated, as shown by Kustowski *et al.* (2007). This suggests that crustal corrections subtracted from the data account for the biggest crustal effect. We recognize that variations in crustal thickness in Eurasia have a non-linear effect on the data and apply non-linear corrections to the measured surface-wave phase anomalies, body-wave traveltimes and in the calculation of synthetic seismograms, as described in Kustowski *et al.* (2007). The mantle is, however, parametrized in our model up to a constant depth of the Moho located at 24.4 km depth, as in our 1-D reference model STW105 (Kustowski *et al.* 2008).

Since the resolving power of our data in the lower mantle is not as good as in the upper mantle, we aim to determine regional-scale heterogeneity in Eurasia only above the 650-km discontinuity. To avoid numerical instabilities associated with the transition from the finely parametrized upper mantle to the coarsely parametrized lower mantle, the high-resolution part of the model is constrained by the parametrization to vanish at 650 km. The sensitivity of the data to the heterogeneity in the lower mantle and topography of the transition zone discontinuities is accounted for by removing predictions of S362ANI from the data vector. Finer-scale anisotropic variations are defined only for four B-splines since we have not found strong evidence for significant radial anisotropy below ∼200–250 km, as discussed in Kustowski *et al.* (2008).

The total number of coefficients defining our new model of Eurasia is 21 967, but we invert only for the 14 003 unknowns corresponding to the fine parametrization in Eurasia. The remaining 7964 coefficients are fixed to the values defined in the global model S362ANI, as discussed in Section 2.3. The total number of free parameters is relatively small because we confined the high-resolution isotropic perturbations to the upper mantle, and we used only four radial splines to parametrize the anisotropic variations. In contrast, Nettles & Dziewoński (2008) inverted simultaneously for the $v_{SH}$ and $v_{SV}$ variations extending into the lower mantle in both the high- and low-resolution regions. Consequently, their North America model, which has the same lateral nominal resolution and nearly the same vertical nominal resolution as ours, comprises ∼17 200 coefficients, that is, almost as many as our model despite the much smaller area of the region with fine parametrization.

### 2.3 Inversion

We invert for the finely parametrized model of Eurasia S2.9EA as a perturbation with respect to the coarsely parametrized 3-D global starting model S362ANI. We incorporate the coefficients $\boldsymbol{m}^{\mathrm{S362ANI}}$ of the global model as a part of a new 3-D model

$$\boldsymbol{m}^{\mathrm{3D}} = \begin{pmatrix} \boldsymbol{m}^{\mathrm{S362ANI}} \\ \boldsymbol{m}^{\mathrm{eura}} \end{pmatrix}, \tag{1}$$

where the coefficients $\boldsymbol{m}^{\mathrm{eura}}$ correspond to the finer parametrization in Eurasia shown in Fig. 2. The sensitivity matrix $\mathbf{A}$ for all data is calculated using the 1-D reference model STW105 (Kustowski *et al.* 2008) for the $\boldsymbol{m}^{\mathrm{3D}}$ parametrization. The radial sensitivity of surface waves and waveforms is determined from the eigenfunctions of normal modes of the Earth, and we use the great circle approximation to calculate the lateral sensitivities. For waveforms, we take advantage of the path-average approximation of Woodhouse & Dziewonski (1984). Body-wave traveltimes are analysed using ray theory. Inner-product matrices $\mathbf{A}^T\mathbf{A}$ and data vectors $\mathbf{A}^T\mathbf{d}$ corresponding to each data set are added with weights selected in such a way that different radial splines are constrained as uniformly as possible. In addition, we give high-quality data higher weights in the inversion. For surface waves, the quality is determined based on the variance calculated for rays travelling along similar paths and for waveforms by the root-mean-square misfit.

To correct the data vector using predictions of S362ANI, we define a starting model

$$\boldsymbol{m}_0^{\mathrm{3D}} = \begin{pmatrix} \boldsymbol{m}^{\mathrm{S362ANI}} \\ \mathbf{0} \end{pmatrix}. \tag{2}$$

The predictions of $\boldsymbol{m}_0^{\mathrm{3D}}$ are subtracted from the observed data vector $\mathbf{A}^T\mathbf{d}^{\mathrm{obs}}$ and then the corrected data vector

$$(\mathbf{A}^T\mathbf{d})^{\mathrm{cor}} = \mathbf{A}^T\mathbf{d}^{\mathrm{obs}} - \mathbf{A}^T\mathbf{A}\boldsymbol{m}_0^{\mathrm{3D}} \tag{3}$$

is inverted in the least-squares sense for the high-resolution perturbations

$$\boldsymbol{m}^{\mathrm{eura}} = (\mathbf{A}^T\mathbf{A} + \mathbf{D}^T\mathbf{D})^{-1}(\mathbf{A}^T\mathbf{d})^{\mathrm{cor}}. \tag{4}$$

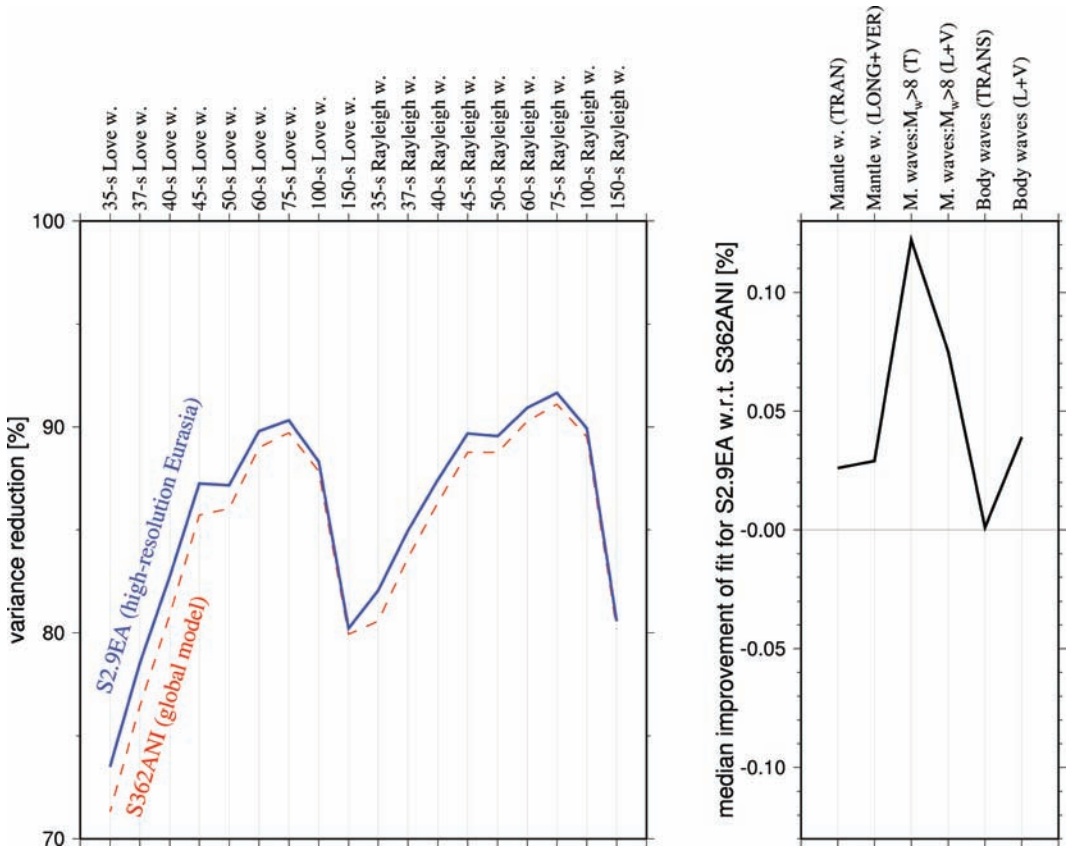


**Figure 4.** Variance reduction for S2.9EA and S362ANI. The variance reduction for surface-wave phase anomalies is shown on the left-hand side. For waveforms, the improvement in the variance reduction is very small but systematic and only the median improvement for each type of waveforms is plotted. LONG, TRAN and VERT indicate longitudinal, transverse and vertical components of a seismogram, respectively.

The damping matrix **D** minimizes the vertical and horizontal roughness of $\boldsymbol{m}^{\text{eura}}$ with respect to S362ANI. For the spline parametrization, the damping matrices have to be calculated numerically. As mentioned before, because of excellent ray path coverage in Eurasia, the choice of the regularization technique does not play an important role in our inversion.

We solve eq. (4) using the Cholesky decomposion (Trefethen & Bau 1997). The final model describing perturbations with respect to STW105 at a given depth $d$, co-latitude $\theta$ and longitude $\phi$ is defined as a sum $\boldsymbol{m}^{\text{S362ANI}}(d, \theta, \phi) + \boldsymbol{m}^{\text{eura}}(d, \theta, \phi)$.

Initially, we calculated a model $\boldsymbol{m}^{\text{3D}}_{SW}$ by performing a computationally inexpensive linear inversion of only surface wave data to get as close to the final, high-resolution solution as possible. The model $\boldsymbol{m}^{\text{3D}}_{SW}$ was then used to calculate synthetic seismograms and partial derivatives for the waveform inversion, which requires more computations. Then, the surface wave, waveform and traveltime data were inverted jointly for the final model S2.9EA.

The solution of eq. (4), that is, the high-resolution perturbations with respect to the global model, are shown in Fig. 3(b) for the depth of 90 km. These perturbations have shorter wavelengths and are not correlated with the velocity anomalies in the global model (Fig. 3a). This suggests that the inversion revealed structures that had not been modelled in S362ANI due to a coarse parametrization rather than due to excessive damping in Eurasia. When the high-resolution perturbations are added to the global model, they reveal more small-scale details (Fig. 3c). The question whether small-scale structures can be resolved is often addressed by checkerboard tests. Such tests, however, cannot demonstrate the ability of the inversion to resolve structures of certain wavelength because they assume that theory used to calculate the sensitivity kernels is perfect. We think that it is more instructive to discuss whether known tectonic features are imaged in our model and whether our model shows structures observed in earlier, often higher-resolution studies. For example, in S362ANI, the East European Craton appears as one fast-velocity anomaly at 90 km depth while in S2.9EA, the anomalies beneath the Urals and Baltic Shield are clearly separated from each other. Slow-velocity anomalies in tectonically active regions are better correlated with surface tectonics in S2.9EA than in S362ANI. The boundary between low and high velocities beneath Tibet and India, respectively, is aligned with the plate boundary in S2.9EA; the alignment is poor in the global model. In Section 3, we will also show that many of the regional-scale anomalies in our model have been previously reported in earlier high-resolution studies involving *P*-wave tomography and receiver functions. Some of the structures unveiled through the regional inversion are as narrow as ∼500 km and we expect to resolve anomalies of this size based on theoretical work of Yoshizawa & Kennett (2002) and Sieminski *et al.* (2004). The latter mentioned that a regional-scale resolution can be achieved if appropriate regularization is used, however, our experiments show that the ray path coverage in Eurasia is so good that the choice of the regularization scheme does not significantly affect the model.

The addition of the smaller-scale anomalies in S2.9EA lead to an improved fit to the data compared with that of the starting model S362ANI (Fig. 4). The additional reduction of normalized variance

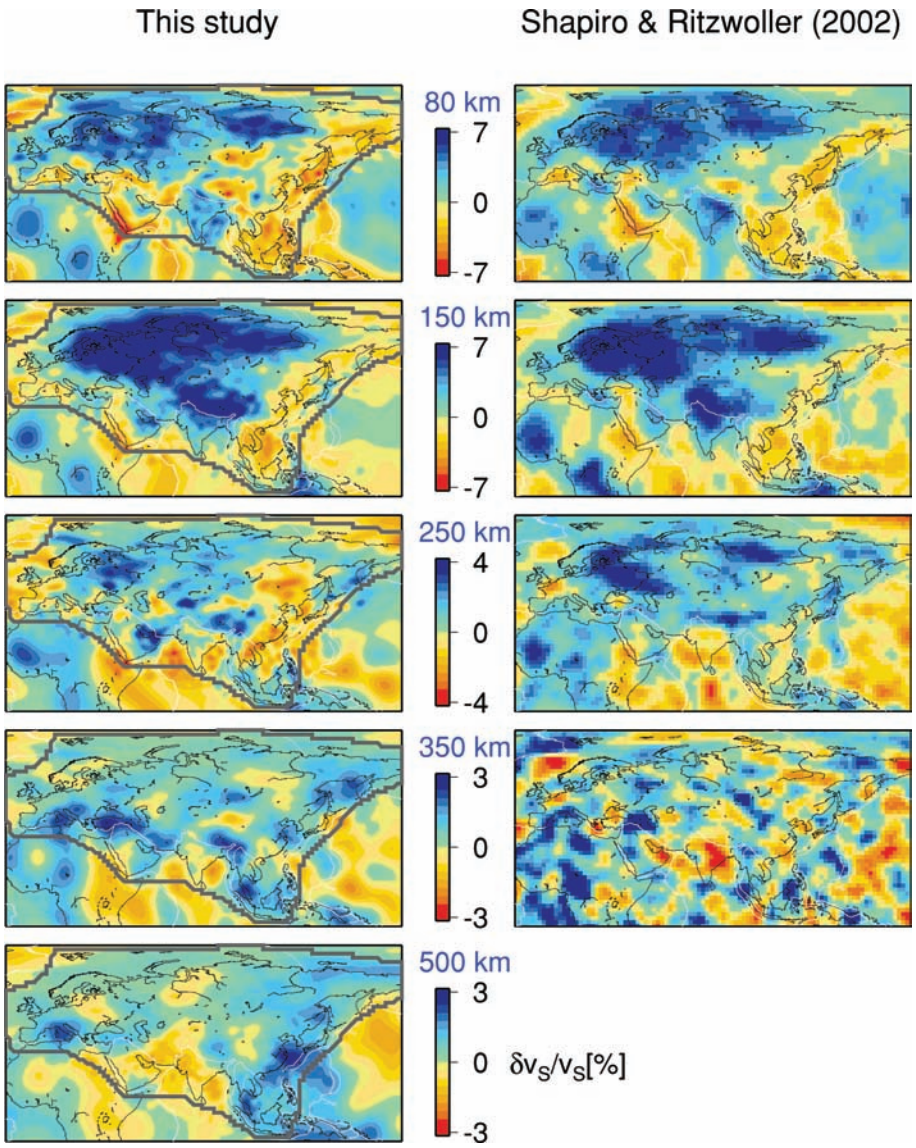


**Figure 5.** Shear-wave velocity variations in our model S2.9EA (left-hand side) and CU_SRT1.0 of Shapiro and Ritzwoller (2002, right-hand side). The variations $\delta v_S/v_S = (\delta v_{SH}/v_{SH} + \delta v_{SV}/v_{SV})/2$ in S2.9EA are calculated with respect to the reference model STW105 (Kustowski *et al.* 2008) and plotted after removing the global average. The variations in CU_SRT1.0 are defined as $\delta v_S/v_S$, where $v_S = (v_{SH} + v_{SV})/2$ and plotted with respect to the average velocity at each depth. White lines indicate plate boundaries and grey line shows the model region.

is about 2 per cent for the shortest-period surface waves and somewhat less for longer-period waves. For the waveform data sets, the improvement in data fit is systematic, but small, which is to be expected since most of the residual variance is due to noise and unmodelled amplitude anomalies.

Short-wavelength anomalies (Fig. 3b), which correspond to spherical-harmonic degrees ∼19–72, show several times lower amplitudes than the amplitudes of the long-wavelength anomalies corresponding to degrees up to 18 (Fig. 3a). This is consistent with the predominance of long-wavelength heterogeneity patterns in the mantle, suggested by Su & Dziewonski (1991) and with the decrease in the amplitude power with wavelength reported by Chevrot *et al.* (1998), but contradicts the earlier results of Passier & Snieder (1995), which suggested that the short-wavelength anomalies in global models were suppressed due to the truncation of the spherical harmonic expansion.

We have performed a number of experiments to explore the possible errors in the model, but we do not present a quantitative error analysis in the paper. Difficulties of different techniques used to evaluate formal model errors are summarized by Shapiro & Ritzwoller (2002). These authors test a new and interesting method to measure model uncertainty using a Monte Carlo method, which overcomes some of the difficulties; it is, however, still sensitive to a number of *a priori* assumptions.

## 3 VELOCITY STRUCTURE BENEATH EURASIA

In Fig. 5, we compare our model S2.9EA with the model CU_SRT1.0 of Shapiro and Ritzwoller (2002). CU_SRT1.0 was obtained from surface-wave group- and phase-velocity measurements. It is a global model parametrized in terms of $2^\circ \times 2^\circ$ blocks, which offer a

similar nominal resolution to our spline parametrization with 2.9° spacing. Shapiro & Ritzwoller (2002) focus their interpretation on Eurasia, where the data coverage is best. To date, no other model encompassing the entire Eurasia with regional-scale detail has been presented.

We emphasize two differences between S2.9EA and CU_SRT1.0. The latter is well constrained by surface waves only within the uppermost 200–250 km of the mantle, whereas long-period waveforms incorporated in this study provide additional constraints on the structures at larger depths. The comparison between the two models should therefore demonstrate the merit of combining diverse data sets in the determination of the deeper part of the upper mantle. Second, we correct our data for crustal effects using CRUST2.0 (Bassin *et al.* 2000) and parametrize the mantle model up to a constant depth of 24.4 km, whereas Shapiro & Ritzwoller (2002) start their analysis with a modified version of CRUST5.1 (Mooney *et al.* 1998) and allow for variations in the depth of the Moho to fit their data. By comparing S2.9EA with CU_SRT1.0, we may identify robust velocity anomalies in the mantle that do not depend strongly on the differences in the crustal structure.

At 80 km, slow-velocity anomalies are less pronounced and fast-velocity anomalies have a larger extent in CU_SRT1.0 compared with S2.9EA. This implies that Eurasian averages relative to global averages are slightly different in the two models. Otherwise, the distribution and amplitudes of lateral velocity variations are very similar. The models have a comparable resolution; the shortest-wavelength anomalies are slightly narrower in S2.9EA. The most pronounced features at a depth of 150 km are fast-velocity anomalies beneath the East European Platform, Siberia and Tibet, which nearly vanish at a depth of 250 km. At 350 and 500 km, our model is dominated by a band of fast velocities beneath the Mediterranean Basin, Turkish Plateau, Tibet and the subduction zones in the southeastern and eastern Eurasia. These anomalies have amplitudes of up to 3 per cent and are correlated with the distribution of regions of current and past tectonic convergence. They are also observed in tomographic models constrained by surface (Boschi *et al.* 2004) and body waves (Spakman *et al.* 1993) and may represent the subducted lithosphere, as predicted by the tectonic reconstruction of the Mediterranean basin (de Jonge *et al.* 1994), or downwellings beneath orogenic regions (Tilmann *et al.* 2003). Shapiro & Ritzwoller (2002) state that below 250 km depth the uncertainties in their model tend to be larger than amplitudes of the velocity anomalies. At 350 km, CU_SRT1.0 shows short-wavelength anomalies with amplitudes up to 8 per cent, which are unlikely to represent true mantle structures as the sensitivity and resolution of surface waves diminish below 200 km. We think that our model is more robust in this depth range.

The correlation between the two models in Eurasia is as high as 0.87 at 80 km, 0.91 at 150 km and 0.75 at 200 km, suggesting that velocities at these depths are very well constrained by surface waves. At larger depths, CU_SRT1.0 is not well constrained and the correlation is only 0.51 at 250 km and 0.21 at 350 km. However, the dramatic decrease in the strength of the anomalies between 150 and 250 km is observed in both models. Different approaches used to account for the crustal structure appear to affect the velocity patterns appreciably only at very shallow depths in the mantle as the correlation at 50 km is still as high as 0.67.

Fig. 6 shows vertical cross-sections through different parts of Eurasia in S2.9EA. Our goal is to demonstrate that regional-scale structures, discussed in a number of regional, often higher-resolution studies, can also be found in this continental-scale model. In cross-section A–A′, positive anomalies between depths of 100 and 200 km are very strong and nearly vanish below 250 km. The presence of strong, fast-velocity anomalies down to ∼200 km is consistent with the model of Priestley & Debayle (2003), who inverted surface wave data for shear wave velocities beneath Siberia. However, a continental-scale model is necessary to demonstrate that these anomalies extend over ∼7000 km from the East European Craton to Siberia. The presence of a negative $\partial v_S/\partial depth$ (hereafter $\partial v_S/\partial h$) gradient underlying a fast-velocity lid is consistent with the study of Grand & Helmberger (1985), although in S2.9EA it is located at a slightly larger depth. A discontinuity associated with a compressional-velocity decrease at a depth of ∼200 km in the East European Craton and Western Siberia was also reported in 2-D models of Ryberg *et al.* (1996) and Morozova *et al.* (1999). The strong gradient zone underlying the fast-velocity layer beneath continents will be further discussed in Section 4.

Cross-section B–B′ shows the structure beneath the Turkish plateau. A tomographic image of this region, constrained by surface waves, was recently obtained by Maggi and Priestley (2005). They reported the presence of a slow-velocity anomaly, perhaps related to the partial delamination of the lithosphere, extending ∼200 km into the mantle. Our model also shows slower-than-average velocities in this region, however, only down to a depth of 100–150 km. While the model of Maggi & Priestley (2005) does not extend west of the Aegean, S2.9EA shows the east-dipping subduction beneath the Hellenic Arc, which was also found in the tectonic reconstruction of de Jonge *et al.* (1994) and the compressional-wave velocity model of the Mediterranean of Spakman *et al.* (1993). Whereas the slow-velocity structures in the model of Maggi & Priestley (2005) vanish below 200–250 km depth, in our model, they are underlain by a fast-velocity region connected with the subduction zone beneath the Hellenic Arc. The fast velocities may represent cold, subducted material as the exothermic 410-km discontinuity is elevated.

Cross-section C–C′ cuts two pronounced, shallow, slow-velocity regions in eastern Eurasia. The easternmost anomaly is associated with the backarc extension beneath the Sea of Japan and is underlain by the subducted Pacific lithosphere, characterized by fast velocities. The depression of the 650-km discontinuity in this region likely results from the subhorizontal deflection or accumulation of the subducted material in the transition zone (Shearer & Masters 1992; Gu *et al.* 1998, 2003). The second shallow, slow-velocity region in C–C′ is located beneath the Altai Mountains, and it is underlain by another slab-like structure. A fast-velocity anomaly at this location, whose deeper part might be attributed to the closing of the Mongol-Okhotsk Ocean, was previously described by van der Voo *et al.* (1999).

Cross-section D–D′ shows the velocity structure beneath Tibet and approximate depths of reflectors taken from Kumar *et al.* (2006), who analysed receiver functions along the D–D′ line. The reflector associated with the velocity decrease at ∼200 km is well aligned with the zone of a strong gradient in the southern part of the cross-section. The tomographic model, however, does not capture an abrupt change in the depth of the reflector observed in the receiver functions. Kumar *et al.* (2006) attribute the reflections to the base of the subducted Indian lithosphere in southern Tibet and Asian lithosphere in northern Tibet. Both S2.9EA and the receiver functions show that this boundary is inclined at a shallow angle in northern Tibet and a steeper angle in southern Tibet, and has an approximately constant depth beneath central Tibet. However, the strongest gradients in central and northern Tibet are observed at a slightly larger depth than the reflector.

The interpretation of the shallowest 100 km in our model should be carried out with caution because of a simplified parametrization.

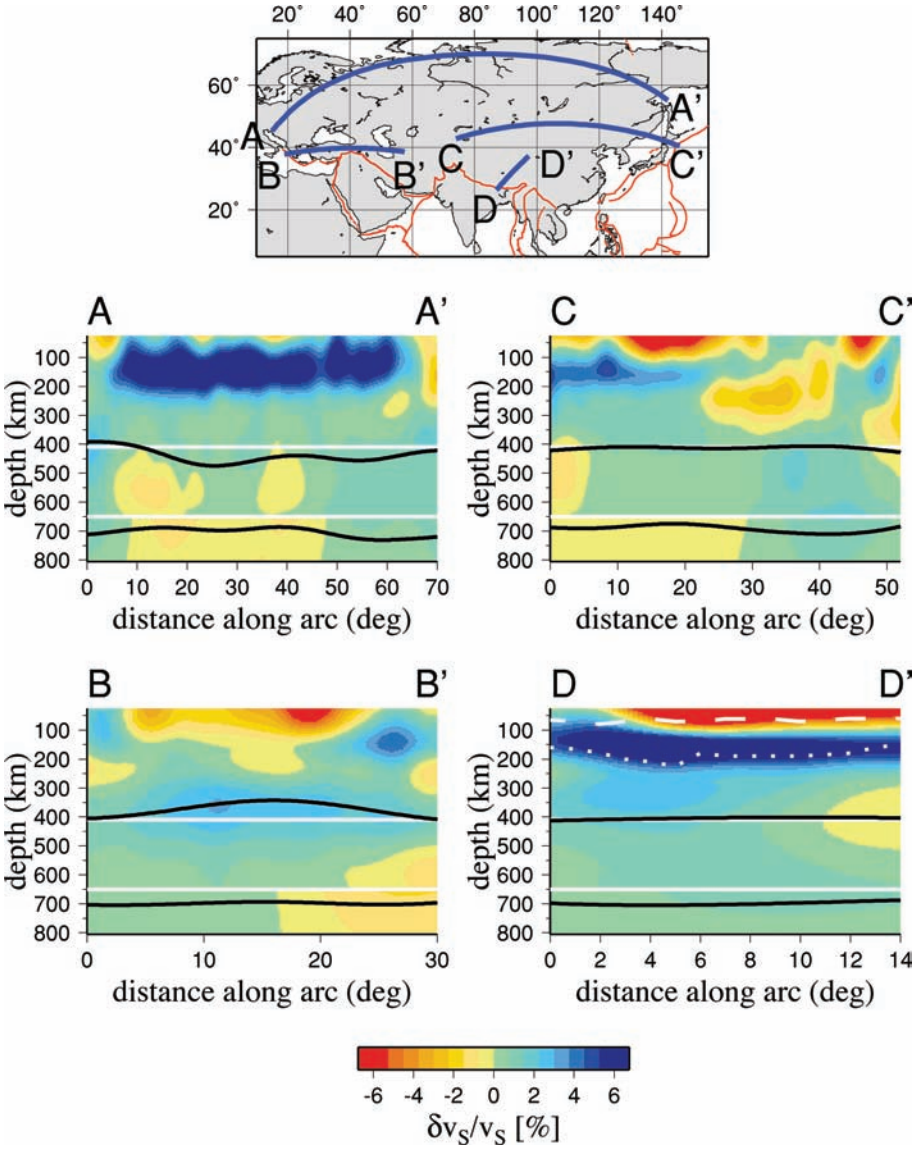


**Figure 6.** Vertical cross-sections through S2.9EA. The blue lines in the uppermost panel indicate the location of the cross-sections. The velocity perturbations $\delta v_S/v_S$ are plotted with the global average removed. The white solid lines indicate the 410 and 650 km depths. The black lines represent the topographies of the transition zone discontinuities plotted with the five-fold exaggeration. The white dashed and dotted lines are approximate depths of the Moho and lithosphere–asthenosphere boundary, respectively, taken from Kumar *et al.* (2006).

Regardless of the parametrization, the depth of strong positive $\partial\delta v_S/\partial h$ gradients in central and northern Tibet is consistent with the depth of the reflector associated with the velocity increase, reported by Kumar *et al.* (2006) as the Moho, and with the depth of the gradients in CU_SRT1.0, as shown in Kustowski (2007). The shallow slow-velocity layer vanishes near the southern end of D–D′, whereas the receiver functions become complex and the reflector was interpreted by Kumar *et al.* (2006) to be at roughly the same depth as beneath central Tibet.

## 4 BASE OF THE CONTINENTAL LITHOSPHERE?

The amplitudes of fast-velocity anomalies in northern Eurasia dramatically decrease between depths of 150 and 250 km (Fig. 6), but velocities increase in this depth range in the 1-D reference model STW105, as well as in PREM. It is therefore instructive to compare the relative velocities in the 3-D model S2.9EA with the absolute ones. The gradient in the anomalies at ∼200 km is so strong that it leads to decrease in the absolute velocity with depth (Fig. 7). This behaviour is also observed in the starting, global model S362ANI and therefore cannot be attributed to the inversion for the continental model. The presence of strong gradients in not only relative, but also in absolute velocities, provides an additional indication of a dramatic change near 200-km depth. Our long-period data, however, do not have enough resolution to discriminate between a gradient zone and a discontinuity.

The two panels at the bottom of Fig. 7 compare the global model S362ANI, calculated using STW105 as the 1-D reference model, with a model S362ANI_PREM, based on the reference model PREM. Otherwise, the two models were obtained using the same data and technique and show nearly identical lateral velocity

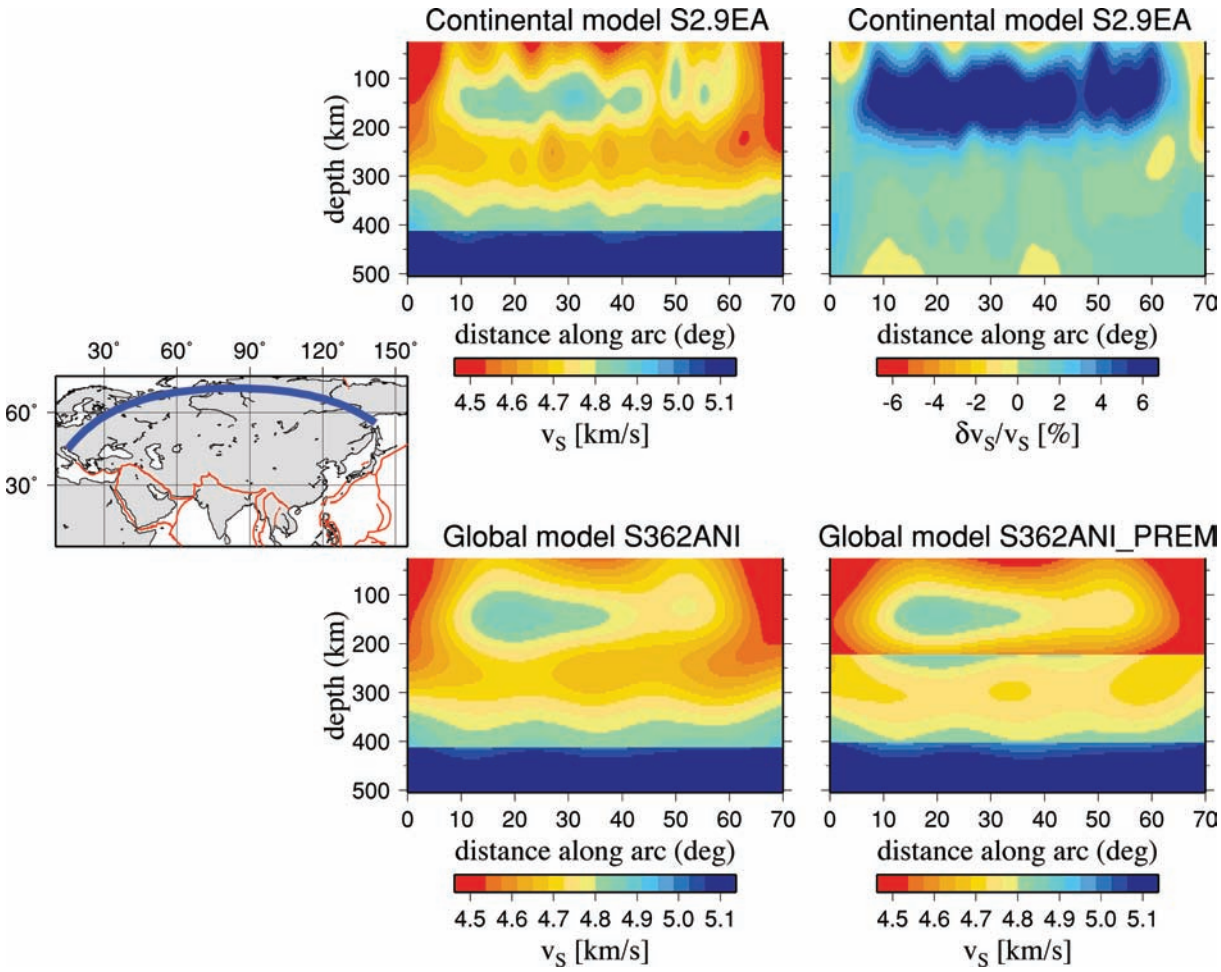


**Figure 7.** Vertical cross-sections through the upper mantle in northern Eurasia, calculated along the arc indicated with the blue line in the left-hand panel. The red contours on the map delineate plate boundaries. Upper panels: absolute (centre) and relative (right-hand side) velocities in the continental model S2.9EA, which was derived using STW105 (Kustowski *et al.* 2008) as the reference model. Lower panels: absolute velocities in S362ANI (centre) calculated as a perturbation with respect to STW105 and in a similar model S362ANI_PREM (right-hand side) calculated as a perturbation with respect to PREM. The absolute velocities are defined as $v_S = (v_{SH} + v_{SV})/2$. The perturbations are defined as $\delta v_S/v_S = (\delta v_{SH}/v_{SH} + \delta v_{SV}/v_{SV})/2$ and plotted with the global average removed.

variations. The absolute velocity structure in S362ANI_PREM is characterized by the positive $\partial v_S/\partial h$ discontinuity at 220 km, as in PREM. The 3-D inversion, however, forced the velocities to decrease between 150 and 220 km and between 220 and 300 km. The velocity jump at 220 km in PREM, therefore, appears to be inconsistent with the data in northern Eurasia. This suggests that the absolute velocity gradients in this region cannot not be resolved properly if PREM is used as a reference model.

Gu *et al.* (2001b) performed a global survey of shear waves reflected from the bottom of the hypothetical 220-km discontinuity. They showed that the $S_{220}S$ seismogram predicted by PREM does not match the observed seismogram with the bounce point beneath Siberia. Gu *et al.* (2001b) recognized that this discrepancy may result from either the topography of the discontinuity or reversed polarity of the reflector. The latter interpretation is consistent with the decrease in velocity observed in S2.9EA. Even if the reflector was not a discontinuity, it would be expected to produce a significant arrival in the long-period data analysed by Gu *et al.* (2001b), which are not capable of distinguishing between the discontinuity and a 50-km thick gradient zone.

Further indications of the presence of the negative $\partial v_S/\partial h$ gradient or discontinuity at ∼200 km is found in regional seismic studies from northern and central Eurasia. 1-D models of compressional-wave velocities of Mechie *et al.* (1993) show a discontinuity at 200–250 km underlain by a local velocity minimum. The discontinuity at ∼200 km along the seismic profile 'Quartz' was interpreted by Ryberg *et al.* (1996) as the lithosphere–asthenosphere boundary, and a similar discontinuity can also be found in the model of Morozova *et al.* (1999). Local compressional-wave velocity minima at 200–250 km beneath seismic profile 'Kraton' were reported by Nielsen & Thybo (1999). Grand & Helmberger (1985) showed that the shield model SNA (Grand & Helmberger 1984) with the strong negative gradient between 150 and 200 km fits the multiply-reflected shear waves in central and northern Eurasia.

Given our results and the earlier studies, it is tempting to infer the presence of a major boundary at ∼200 km beneath cratons in Eurasia, perhaps associated with the transition from the lithosphere to the asthenosphere. Priestley & Debayle (2003) call the ∼200-km-thick fast-velocity layer beneath Siberia a seismic lithosphere, which is likely to be somewhat thicker than the thermal

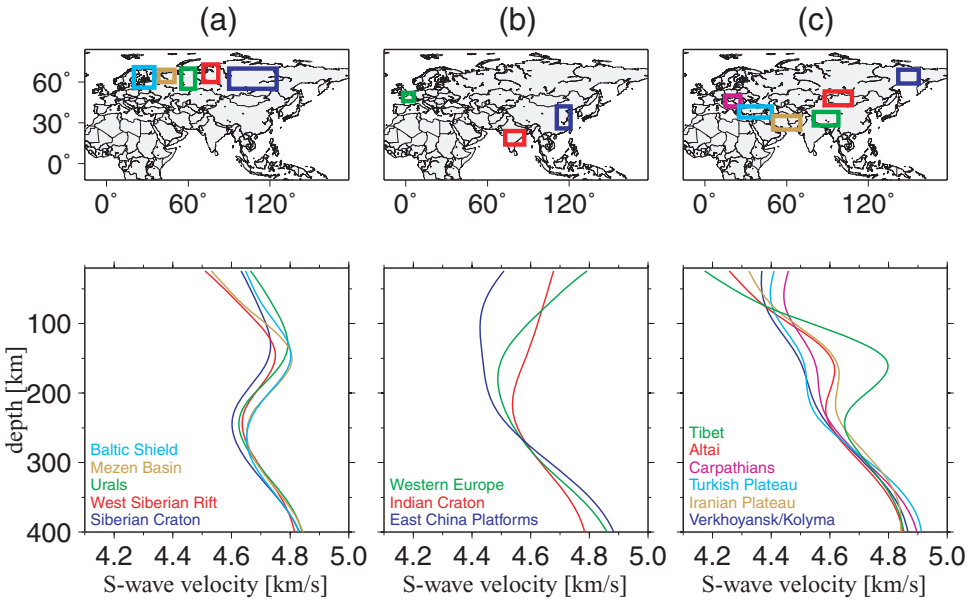


**Figure 8.** Vertical profiles of the Voigt average shear wave velocity. The velocities plotted in the lower panels represent averages calculated within rectangular regions shown in the upper panels. The names and geographical extent of particular cratons and sedimentary basins can be found, for example, in Enkin *et al.* (1992), Yin & Harrison (1996) and Nikishin *et al.* (1996). (a) Northern Eurasia. (b) Regions, which are not characterized by the zone of negative $\partial v_s/\partial h$ gradient at ∼200 km. (c) Regions of present or past tectonic activity.

lithosphere, defined as a conductive boundary layer (Jaupart & Mareschal 1999). However, Lerner-Lam & Jordan (1987) found that Rayleigh-wave data require the velocity structures beneath northern Eurasia and western Pacific to differ down to a depth of 400 km. The fast-velocity layer in northern Eurasia appears to be thicker than 300 km also in some global tomographic models (e.g. Megnin & Romanowicz 2000; Gu *et al.* 2001a). Perturbations in S2.9EA are indeed positive down to 400 km beneath cratons in Eurasia, but they are weak (+1 to +2 per cent) below 250 km, whereas up to +9 per cent anomalies are observed at 150 km depth. In an attempt to reconcile the apparently contradictory results, we speculate that the ∼200-km-thick layer of strong fast velocity anomalies may be the continental lithosphere, the conductive boundary layer, whereas the weaker anomalies extending down to 400 km may be attributed to a continental root. The root may represent a region of increased viscosity in the asthenosphere due to low temperatures beneath continents (Shapiro *et al.* 1999) or a compositionally buoyant mantle, depleted in heavy elements (Jordan 1975, 1978). Strong velocity gradients favour compositional boundaries, however, a quantitative study is needed to support such an interpretation. We also note that thick layers of strong, fast-velocity anomalies reported in some older tomographic models may be, to some extent, an artefact of using less accurate, linear crustal corrections in the waveform inversion, as demonstrated by Kustowski *et al.* (2007). Thinner, 200–250-km-thick, layers of significantly faster-than-average velocities beneath cratons are observed in more recent global models of Ritsema *et al.* (2004), Panning & Romanowicz (2006) and Kustowski *et al.* (2008) in which non-linear crustal corrections were implemented.

It is not possible to estimate precisely the depth of the boundary near the bottom of the lithosphere, based on our tomographic model. We can, however, infer from Fig. 7 that the strongest vertical gradients beneath the East European Craton are 20–30 km deeper than beneath Siberia and 40–50 km deeper than beneath the West Siberian Rift. This is consistent with the estimates of the lithospheric thickness of Priestley & McKenzie (2006), who combined a seismological and thermal model of the oceanic lithosphere, accounted for the compositional difference in the continental lithosphere and used kimberlite data to test the velocity–temperature relationship for the continents. Much larger variations in thickness, however, were reported by Artemieva & Mooney (2001). These authors analysed heat flow data and found that the thermal lithosphere may be as thick as ∼350 km beneath Siberia, ∼175–300 km thick beneath the East European Craton and as thin as ∼125 km beneath the West Siberian Rift.

To investigate the lateral extent of the gradient zone at a depth of 200 km, we plot vertical velocity profiles at different locations in Eurasia (Fig. 8) and beneath different continents and in different models (Fig. 9). The profiles beneath sedimentary basins and rift systems in northern Eurasia, as well as beneath the Urals, show the same decrease in velocity between 150 and 250 km as those beneath cratons (Fig. 8a). This similarity indicates that the boundary may be located at similar depths, regardless of differences in the shallow structure. The steep gradient zone at ∼200 km however is not observed in some other, relatively stable parts of the continent (Fig. 8b), but it is present beneath Tibet and Altai (Fig. 8c). The 150–250 km depth range is also anomalous in other tectonically active regions; velocities increase with depth but at a slower rate compared with the overlying and underlying mantle.

Figs 9(a) and (b) show velocity profiles in different models for cratons in Eurasia and North America—the two continents best sampled by surface waves. We included only models that have been obtained independent of PREM, that is, without a discontinuity imposed at 220 km. The negative gradient zone at ∼200 km beneath northern Eurasia and the Canadian Shield is observed not only in S2.9EA but also in CU_SRT1.0 and SNA (Grand & Helmberger 1984). The velocity profile beneath Canada in our model, although somewhat smoother, is remarkably similar to SNA, a model derived from multiply reflected body waves. A strong positive gradient is observed in northern Eurasia, down to 150 km in S2.9EA and CU_SRT1.0. The latter also shows the shallow positive gradient

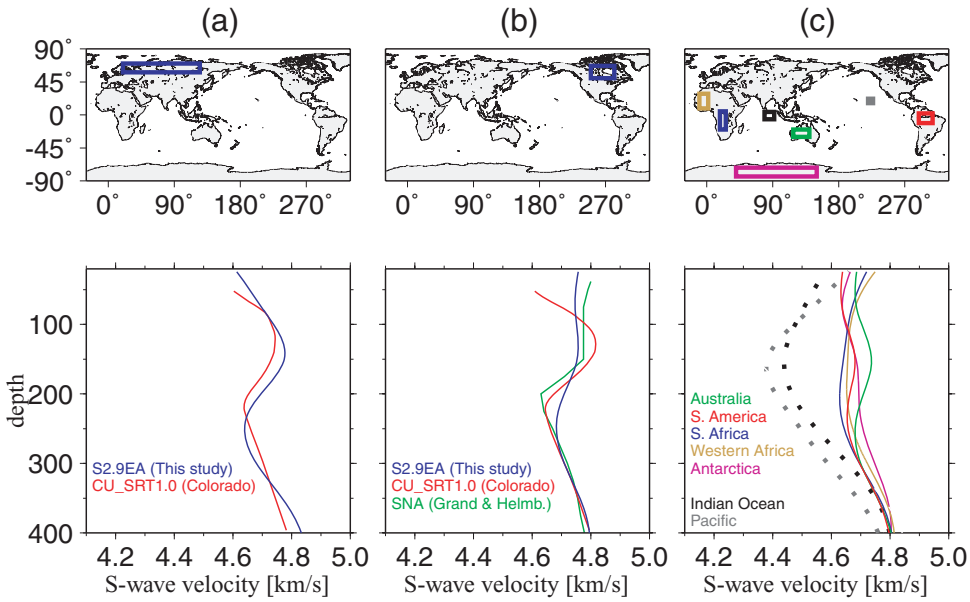


**Figure 9.** Vertical profiles of the Voigt average shear wave velocity beneath (a) northern Eurasia and (b) Canadian Shield in S2.9EA, CU_SRT1.0 and SNA (Grand & Helmberger 1984). (c) Velocity profiles for cratons outside of Eurasia (solid lines) and beneath oceans (squares) in S2.9EA.

beneath the Canadian Shield; however, no strong gradients are found in our model and in SNA.

In S2.9EA, the velocity decrease between 150 and 250 km is also observed beneath cratons in South America and Australia (Fig. 9c), suggesting that 175–225 km might be a typical depth of the boundary in stable continental settings. The negative gradients at 200 km are, however, not observed beneath Antarctica and Africa. Stable parts of different continents show remarkably similar velocities, which are confined to the 4.6–4.75 km s$^{-1}$ range down to ∼300 km. The comparison with the oceanic regions demonstrates that small differences between the continental and oceanic regions extending to at least 300 km may exist; however, they do not rule out the presence of the lithospheric base at 200 km.

## 5 VARIATIONS IN RADIAL ANISOTROPY

We compare S2.9EA with a simpler version of the model, S2.9EA_ISO, in which high-resolution anisotropic variations are not inverted for and the low-resolution anisotropic variations are fixed to those in the global model S362ANI (Fig. 10). Long-wavelength anisotropic patterns in the two models are similar. Shorter-wavelength anisotropic anomalies are found in S2.9EA. However, the differences between the two models are not clearly correlated with any tectonic features in Eurasia.

We do not discuss the anisotropic part of our model further because we think that radial anisotropy in the upper mantle is still difficult to constrain. In Kustowski *et al.* (2008), we demonstrate that, with the exception of few regions, radial anisotropy is poorly correlated in different models with highly correlated isotropic variations. This is consistent with the results of Shapiro & Ritzwoller (2002), who conclude that uncertainty of the anisotropic variations in their model is very high.

Although anisotropy is difficult to constrain, velocity-anisotropy trade-offs for short-wavelength anomalies are small. Fig. 10 demonstrates that the isotropic velocities are not appreciably affected by allowing for high-resolution anisotropic variations, despite the presence of shorter wavelength anisotropic anomales at 100 km and stronger anisotropy at 250 km in S2.9EA, when compared with S2.9EA_ISO.

## 6 CONCLUSIONS

Our new model of Eurasia S2.9EA reveals upper-mantle velocity anomalies narrower than 1000 km and in places as small as ∼300 km. Many of these features are not observed in the starting, low-resolution global model S362ANI and emerged through the inversion for the finely parametrized continental model S2.9EA. We think that these small-scale features reveal real structures because they (1) reduce data misfits, (2) are well aligned with plate boundaries and known tectonic features and (3) are consistent with structures reported in earlier, regional, high-resolution studies. Our results therefore support theoretical predictions, indicating that regional-scale anomalies can be resolved by ray theory based tomography, given good surface-wave data coverage. Whereas earlier high-resolution studies were usually confined to small regions, our new model encompasses the entire Eurasia continent with the regional-scale detail. Because we inverted for this model as a perturbation with respect to the global model, other regional models obtained on top of the same starting model can potentially be compared with Eurasia in a consistent way.

Including mantle- and body-wave waveforms helped us to constrain the deeper upper mantle, which is less well resolved in earlier models such as CU_SRT1.0. The high correlation between our model and CU_SRT1.0 at shallow depths demonstrates that neglecting lateral variations in the Moho depth in the calculation of the sensitivity kernels has small effect on the velocity patterns in the mantle below 80 km depth. This suggests that the biggest effect of the crustal variations on the data was removed by applying the crustal corrections.

The dramatic velocity decrease at ∼200 km beneath northern and central Eurasia, as well as Tibet, is consistent with earlier,

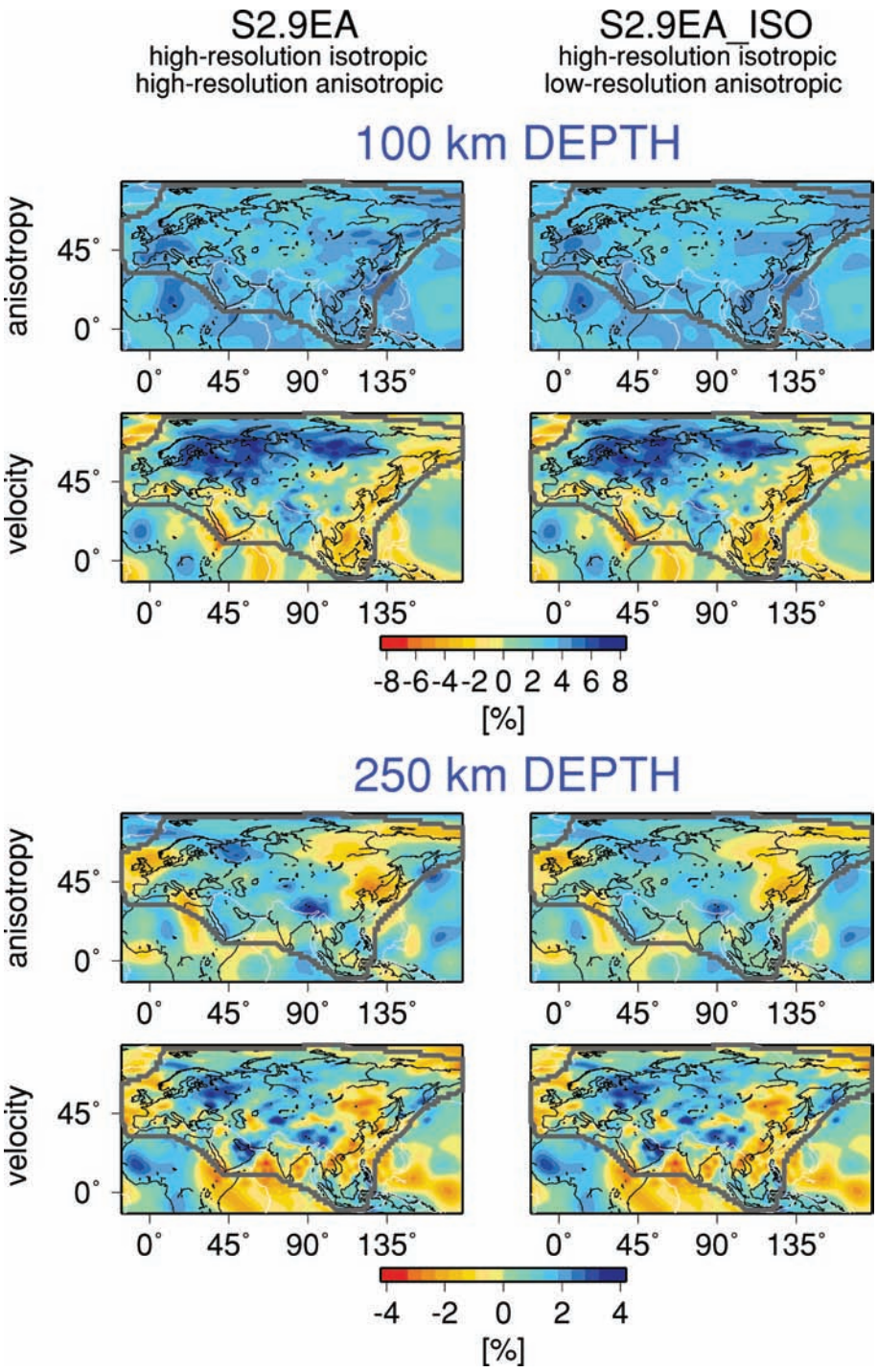


**Figure 10.** Lateral radially anisotropic and isotropic velocity variations in models S2.9EA and S2.9EA_ISO. The former is our preferred model, in which both isotropic and anisotropic high-resolution variations were determined. In model S2.9EA_ISO, only isotropic high-resolution perturbations were inverted for, whereas anisotropic variations are identical to those in the lower-resolution global model S362ANI. The small-scale isotropic variations are not significantly affected by allowing for regional anisotropic variations in the inversion.

high-resolution studies, where it was often interpreted as the base of the lithosphere. In these regions, a layer of up to +9 per cent faster-than-average velocities is underlain by weaker (+1 to +2 per cent) anomalies, extending down to ∼400 km. The weaker anomalies may represent a compositionally distinct continental root or highly viscous asthenosphere beneath cold continents. We cannot rule out that this region is also anisotropic, as proposed by Gung *et al.* (2003); $v_{SH}$ is slightly faster than $v_{SV}$ at 300 km beneath Eurasia in our model. The sharpness of the velocity gradient at ∼200 km depth may favour a vertical compositional boundary, but quantitative studies are needed to test this hypothesis.

The zone of negative $\partial v_S/\partial h$ gradient at ∼200 km is also observed beneath cratons in North America, South America and Australia but not beneath Africa and Antarctica. We find the

lithosphere in Eurasia to be unique in two regards. First, the negative velocity gradients between 150 and 250 km are much stronger than that beneath any other continent, perhaps indicating a sharper boundary. Second, in our model, the positive $\partial v/\partial h$ gradients above 150 km depth are not observed beneath cratons in continents other than Eurasia, in our model. The presence of the negative gradient at ∼200 km is corroborated by CU_SRT1.0 and SNA (Grand & Helmberger 1984), the presence of the positive gradient at shallow depth in northern Eurasia is consistent with CU_SRT1.0 and the lack of strong gradients at shallow depth beneath the Canadian Shield is consistent with SNA. The presence of a negative $\partial v_S/\partial h$ gradient at ∼200 km is observed in a number of independent studies, and we consider it to be robust. On the other hand, the shallow gradient beneath Eurasia is corroborated only by CU_SRT1.0 in which it is observed beneath other continents also.

## ACKNOWLEDGMENTS

This material is based on work supported by National Science Foundation Grants EAR-02-07608 and EAR-06-09111. We thank Nikolai Shapiro and Michael Ritzwoller for making their model available online. Comments from Gabi Laske and two anonymous reviewers helped us improve the manuscript. All figures were made with GMT (http://gmt.soest.hawaii.edu).

## REFERENCES

Artemieva, I.M. & Mooney, W.D., 2001. Thermal thickness and evolution of Precambrian lithosphere: a global study, *J. geophys. Res.,* **106,** 16 387–16 414.

Bassin, C., Laske, G. & Masters, G., 2000. The current limits of resolution for surface wave tomography in North America, *EOS, Trans. Am. geophys. Un.,* **81,** F897.

Boschi, L. & Dziewonski, A.M., 1999. High- and low-resolution images of the Earth's mantle: implications of different approaches to tomographic modeling, *J. geophys. Res.,* **104,** 25 567–25 594.

Boschi, L., Ekström, G. & Kustowski, B., 2004. Multiple resolution surface wave tomography: the Mediterranean basin, *Geophys. J. Int.,* **157,** 293–304.

Chevrot, S., Montagner, J.P. & Snieder, R., 1998. The spectrum of tomographic earth models, *Geophys. J. Int.,* **133,** 783–788.

de Jonge, M.R., Wortel, M.J.R. & Spakman, W., 1994. Regional scale tectonic evolution and the seismic velocity structure of the lithosphere and upper mantle: the Mediterranean region, *J. geophys. Res.,* **99,** 12 091–12 108.

Dziewonski, A.M., 1971. Upper mantle models from 'pure path' dispersion data, *J. geophys. Res.,* **76,** 2587–2601.

Dziewonski, A.M. & Anderson, D.L., 1981. Preliminary reference Earth model, *Phys. Earth planet. Inter.,* **25,** 297–356.

Ekström, G., 2000. Mapping the lithosphere and asthenosphere with surface waves: lateral structure and anisotropy, in *The History and Dynamics of Global Plate Motions*, Vol. 121, pp. 239–255, AGU Geophysical Monograph Series.

Ekström, G., Tromp, J. & Larson, E.W.F., 1997. Measurements and global models of surface wave propagation, *J. geophys. Res.,* **102,** 8137–8157.

Enkin, R.J., Yang, Z., Chen, Y. & Courtillot, V., 1992. Paleomagnetic constraints on the geodynamic history of the major blocks of China from the Permian to the present, *J. geophys. Res.,* **97,** 13 953–13 989.

Garnero, E.J., Helmberger, D.V. & Burdick, L.J., 1992. Preliminary observations from the use of US-soviet joint seismic program data to model upper mantle triplications beneath Asia, *Geophys. J. Int.,* **113,** 252–259.

Grand, S.P. & Helmberger, D.V., 1984. Upper mantle shear structure of North America, *Geophys. J. R. astr. Soc.,* **76,** 399–438.

Grand, S.P. & Helmberger, D.V., 1985. Upper mantle shear structure beneath Asia from multi-bounce *S* waves, *Phys. Earth planet. Inter.,* **41,** 154–169.

Gu, Y.J., Dziewonski, A.M. & Agee, C.B., 1998. Global de-correlation of the topography of transition zone discontinuities, *Earth planet. Sci. Lett.,* **157,** 57–67.

Gu, Y.J., Dziewonski, A.M., Su, W. & Ekström, G., 2001a. Models of the mantle shear velocity and discontinuities in the pattern of lateral heterogeneities, *J. geophys. Res.,* **106,** 11 169–11 199.

Gu, Y.J., Dziewonski, A.M. & Ekström, G., 2001b. Preferential detection of the Lehmann discontinuity beneath continents, *Geophys. Res. Lett.,* **24,** 4655–4658.

Gu, Y.J., Dziewonski, A.M. & Ekström, G., 2003. Simultaneous inversion for mantle shear velocity and topography of transition zone discontinuities, *Geophys. J. Int.,* **154,** 559–583.

Gung, Y., Panning, M. & Romanowicz, B., 2003. Global anisotropy and the thickness of continents, *Nature,* **442,** 707–711.

Jaupart, C. & Mareschal, J.C., 1999. The thermal structure and thickness of continental roots, *Lithos,* **48,** 93–114.

Jordan, T.H., 1975. The continental tectosphere, *Rev. Geophys. Space Phys.,* **13,** 1–12.

Jordan, T.H., 1978. Composition and development of the continental tectosphere, *Nature,* **274,** 544–548.

Kennett, B.L.N., Engdahl, E.R. & Buland, B., 1995. Constraints on seismic velocities in the Earth from travel times, *Geophys. J. Int.,* **122,** 108–124.

Kumar, P., Yuan, X., Kind, R. & Ni, J., 2006. Imaging the colliding Indian and Asian lithospheric plates beneath Tibet, *J. geophys. Res.,* **111,** doi:10,1029/2005JB003930.

Kustowski, B., 2007. Modeling of the anisotropic shear-wave velocity structure in the Earth's mantle on global and regional scales, *PhD thesis*, Harvard University.

Kustowski, B., Ekström, G. & Dziewoński, A.M., 2003. Travel Times in the Regional Distance Range: Results of 3-D Ray Tracing, *EOS, Trans. Am. geophys. Un.,* **84,** S31E–0797.

Kustowski, B., Dziewoński, A.M. & Ekström, G., 2007. Nonlinear corrections for normal-mode seismograms, *Bull. seism. Soc. Am.,* **97,** doi:10.1785/0120070041.

Kustowski, B., Ekström, G. & Dziewoński, A.M., 2008. Anisotropic shear-wave velocity structure of the Earth's mantle: A global model, *J. geophys. Res.,* **113**, B06306, doi:10.1029/2007JB005169.

Larson, E.W.F., Tromp, J., & Ekström, G., 1998. Effects of slight anisotropy on surface waves, *Geophys. J. Int.,* **132,** 654–666.

Lerner-Lam, A.L. & Jordan, T.H., 1987. How thick are the continents?, *J. geophys. Res.,* **92,** 14 007–14 026.

Maggi, A. & Priestley, K., 2005. Surface waveform tomography of the Turkish–Iranian plateau, *Geophys. J. Int.,* **160,** 1068–1080.

Marone, F. & Romanowicz, B., 2007. Non-linear crustal corrections in high-resolution regional waveform seismic tomography, *Geophys. J. Int.,* **170,** doi:10.1111/j.1365-246X.2007.03399.x.

Mechie, J., Egorkin, A.V., Fuchs, K., Ryberg, T., Solodilov, L. & Wenzel, F., 1993. *P*-wave mantle velocity structure beneath northern Eurasia from long-range recordings along the profile Quartz, *Phys. Earth planet. Inter.,* **79,** 269–286.

Megnin, C. & Romanowicz, B., 2000. The three-dimensional shear velocity structure of the mantle from the inversion of body, surface and higher-mode waveforms, *Geophys. J. Int.,* **143,** 709–728.

Mooney, W.D., Laske, G. & Masters, G., 1998. CRUST-5.1: a global crustal model at 5° × 5°, *J. geophys. Res.,* **103,** 727–747.

Morozova, E.A., Morozov, I.B. & Smithson, S.B., 1999. Heterogeneity of the uppermost mantle beneath Russian Eurasia from the ultra-long-range profile QUARTZ, *J. geophys. Res.,* **104,** 20 329–20 348.

Nettles, M., 2005. Anisotropic velocity structure of the mantle beneath North America, *PhD thesis*, Harvard University.

Nettles, M. & Dziewoński, A.M., 2008. Radially anisotropic shear velocity structure of the upper mantle globally and beneath North America, *J. geophys. Res.,* **113,** doi:10.1029/2006JB004819.

Nielsen, L. & Thybo, H., 1999. Seismic tomographic inversion of Russian PNE data along profile Kraton, *Geophys. Res. Lett.,* **26,** 3413–3416.

Nikishin, A.M. *et al.,* 1996. Late Precambrian to Triassic history of the East European Craton: dynamics of sedimentary basin evolution, *Tectonophysics* **268,** 23–63.

Panning, M. & Romanowicz, B., 2006. A three-dimensional radially anisotropic model of shear velocity in the whole mantle, *Geophys. J. Int.,* **167,** 361–379.

Passier, M.L. & Snieder, R., 1995. On the presence of intermediate-scale heterogeneities in the upper mantle, *Geophys. J. Int.,* **123,** 817–837.

Priestley, K. & Debayle, E., 2003. Seismic evidence for a moderately thick lithosphere beneath the Siberian Platform, *Geophys. Res. Lett.,* **30,** doi:10,1029/2002GL015931.

Priestley, K. & McKenzie, D., 2006. The thermal structure of the lithosphere from shear wave velocities, *Earth planet. Sci. Lett.,* **244,** 285–301.

Ritsema, J., van Heijst, H.J. & Woodhouse, J.H., 2004. Global transition zone tomography, *J. geophys. Res.,* **109,** doi:10.1029/2003JB002610.

Ryberg, T., Wenzel, F., Mechie, J., Egorkin, A., Fuchs, K. & Solodilov, L., 1996. Two-dimensional velocity structure beneath northern Eurasia derived from the super long-range seismic profile Quartz, *Bull. seism. Soc. Am.,* **85,** 857–867.

Shapiro, N.M. & Ritzwoller, M.H., 2002. Monte-Carlo inversion for a global shear-velocity model of the crust and upper mantle, *Geophys. J. Int.,* **151,** 88–105.

Shapiro, S.S., Hager, B.H. & Jordan, T.H., 1999. Stability and dynamics of the continental tectosphere, *Lithos,* **48,** 115–133.

Shearer, P.M. & Masters, T.G., 1992. Global mapping of topography on the 660-km discontinuity, *Nature,* **355,** 791–795.

Sieminski, A., Leveque, J.-J.G. & Debayle, E., 2004. Can finite-frequency effects be accounted for in ray theory surface wave tomography, *Geophys. Res. Lett.,* **31,** doi:10.1029/2004GL021402.

Spakman, W., van der Lee, S. & van der Hilst, R.D., 1993. Travel-time tomography of the European-Mediterranean mantle down to 1400 km, *Phys. Earth planet. Inter.,* **79,** 3–74.

Spetzler, J., Trampert, J. & Snieder, R., 2002. The effect of scattering in surface wave tomography, *Geophys. J. Int.,* **149,** 755–767.

Su, W.-J. & Dziewonski, A.M., 1991. Predominance of long-wavelength heterogeneity in the mantle, *Nature,* **352,** 121–126.

Tilmann, F., Ni, J. & INDEPTH III Seismic Team, 2003. Seismic imaging of the downwelling Indian lithosphere beneath central Tibet, *Science,* **300,** 1424–1427.

Trampert, J. & Spetzler, J., 2006. Surface wave tomography: finite-frequency effects lost in the null space, *Geophys. J. Int.,* **164,** 394–400.

Trefethen, L.N. & Bau, D., 1997. *Numerical Linear Algebra*, Soc. Ind. Appl. Math., Philadelphia, PA.

van der Voo, R., Spakman, W. & Bijwaard, H., 1999. Mezozoic subducted slabs under Siberia, *Nature,* **397,** 246–249.

Wang, Z. & Dahlen, F.A., 1995. Spherical-spline parameterization of three-dimensional Earth models, *Geophys. Res. Lett.,* **22,** 3099–3102.

Wang, Z., Tromp, J. & Ekström, G., 1998. Global and local surface-wave inversions: a spherical-spline parameterization, *Geophys. Res. Lett.,* **25,** 207–210.

Woodhouse, J.H. & Dziewonski, A.M., 1984. Mapping the upper mantle: three-dimensional modeling of Earth structure by inversion of seismic waveforms, *J. geophys. Res.,* **89,** 5953–5986.

Yin, A. & Harrison, T.M., 1996. *The Tectonic Evolution of Asia*, Cambridge University Press, Cambridge.

Yoshizawa, K. & Kennett, B.L.N., 2002. Determination of the influence zone for surface wave paths, *Geophys. J. Int.,* **149,** 440–453.

## APPENDIX: MODEL AVAILABILITY

The model of Eurasia S2.9EA is available online at `http://www.seismology.harvard.edu/~kustowsk`.